IEEE Access
Multidisciplinary | Rapid Review | Open Access Journal

Received July 26, 2019, accepted August 11, 2019, date of publication August 22, 2019, date of current version September 5, 2019.

Digital Object Identifier 10.1109/ACCESS.2019.2936872

SSR Analysis of DFIG-Based Wind Farm With VSM Control Strategy

KANGHUI GU[1], (Student Member, IEEE), FENG WU[1], XIAO-PING ZHANG[2], (Senior Member, IEEE), PING JU[1], (Senior Member, IEEE), HAIQIANG ZHOU[1], JIAJIE LUO[2], AND JIANING LI[2], (Member, IEEE)

[1]College of Energy and Electrical Engineering, Hohai University, Nanjing 210098, China
[2]Department of Electronic, Electrical and System Engineering, University of Birmingham, Birmingham B15 2TT, U.K.

Corresponding author: Feng Wu (wufeng@hhu.edu.cn)

This work was supported by a scholarship from the China Scholarship Council (CSC), under Grant 201706710073.

ABSTRACT The wind turbine is usually integrated into the power grid via back to back converter, and the inertia is decreased. Virtual synchronous machine (VSM) control was proposed to improve inertia of the wind farm. While for the doubly-fed induction generator (DFIG)–based wind farm with traditional control strategy, sub-synchronous resonance (SSR) has become a significant problem when it is connected to series compensation transmission lines. Therefore, the impacts of VSM control strategy for DFIG on SSR need to be investigated. In this paper, a detailed small-signal stability analysis model of the VSM control strategy is first established and eigenvalue analysis is then carried out. SSR in the wind farm with the VSM control under different series compensation levels, controller parameters and wind speeds is analyzed, and it is also compared to that in the wind farm with the conventional vector control strategy (VC). Simulations are performed in PSCAD/EMTDC to verify the result of SSR analysis.

INDEX TERMS SSR, VSM, eigenvalue analysis, wind power plant.

I. INTRODUCTION

Wind power generation develops quickly in recent years with global installation of 591 GW by the end of 2018. The installed capacity in China made up nearly 35.7% (211,392 MW), which is much larger than those in USA (96,665 MW) and Europe (189,606 MW) [1]. As the penetration of wind power generation increases, the function of synchronous generators (SG) is weakened and system controllability is gradually lost. Therefore, more and more grid support converters control techniques for the wind turbines have been developed in recent years.

Virtual synchronous machine (VSM) has attracted more and more research interest during the past decade. It was firstly introduced in 2007 [2] in the context of the decrease of the total system inertia due to more and more traditional synchronous generators were replaced by renewable energy generation sources with power electronic converters. By means of mimicking the inertia and damping property of SG through the well-known swing equation, VSM can control the dynamic performance of a renewable energy generator in a similar way as SG does. A better active power-frequency response can be provided for grid-connected converters as well [3]. So far, the concept of VSM has been successfully implemented in real power systems, for instance, the European project VSYNC [4]. VSM is mainly applied in systems with grid-connected voltage source converters (VSC), e.g. full-capacity wind power plants [5], [6], doubly-fed induction generator (DFIG)-based wind farms [7], [8], high voltage DC (HVDC) transmission systems [9], photovoltaic (PV) plants [10] and compensation devices [11], etc. In [5], a synchronverter-based control strategy was proposed for the converters in a PMSG-based system, which has greatly improved the performance of the wind turbine under different system conditions. In [6], a virtual generator control method in combination with a minute-level energy storage was proposed for full capacity converter wind turbines, which has improved the system dynamic response. In [9], based on the synchronverter technique, a parameter tuning method was proposed to emulate SGs by using rectifiers and inverters in a HVDC transmission system. A control strategy was proposed in [10] to make PV plants work like a SG through

The associate editor coordinating the review of this article and approving it for publication was Ke Gu.

energy storage systems, and the transient stability of power systems was successfully enhanced. In [11], VSM concept was extended and successfully applied to STATCOM, which has achieved flexible controls.

Massive penetration of wind power generation has changed the system framework and made the system characteristics become more and more complicated [12]. Sub-synchronous resonance (SSR) is one of the hot topics and has attracted a lot of interests. SSR in wind farms was first presented and discussed in n[13], but didn't attract much attention until the accident happened in the Texas southern power grid in 2009 [14]. The accident was triggered due to a line fault which leads to a radial connection between wind farms and series compensation transmission lines. Since then, similar oscillations were observed in other wind-integrated power systems, e.g., in Buffalo Ridge area of Minnesota [15], in Hebei province in North China [16], etc. Mechanism analysis and mitigation solutions on SSR in DFIG-based wind farms have been carried out in [17]–[24]. These observed oscillations were found similar to induction generator effect (IGE) of thermal power generators [17], which will be triggered when the negative rotor equivalent resistance exceeds the total system resistance under sub-synchronous frequency. This kind of IGE can be affected by different factors, such as series compensation level of transmission lines, wind speed [18], network topology [19] and spatial distribution of wind farms [20]. Particularly, controllers for rotor side converter (RSC) in DFIG play significant roles in SSR. Increase of proportional gain and reduction of integral time constant in proportional integral (PI) controllers will exacerbate system instability [21]. When it comes to SSR mitigation, additional damping controller is usually appended [22]. In this way, converters can continuously track sub-synchronous components and then generate opposite components to damp oscillations. Timely and effective data measurement and transmission among the network are significant in this situation [25], [26]. Additionally, implementation of the flexible ac transmission system (FACTS) devices is also considered to be an effective way to suppress SSR [23], [24].

It has to be mentioned that the DFIG in above SSR research mostly adopts conventional vector control (VC) with phase-locked loop (PLL). How a DFIG with the VSM control behaves in the case of SSR has not been studied. Meanwhile, previous work on the VSM were mostly focused on their superiority on frequency support, rather than certain violent oscillations. The impacts of VSM on SSR need to be further investigated.

In this paper, a DFIG model with a VSM control strategy in a typical SSR system is first presented. Dynamic performance of SSR is then analyzed in comparison with that in the wind farm with conventional VC strategy. The rest of this paper is organized as follows. In section II, a brief description of the wind farm system with VSM or VC control strategy is provided. In section III, a small-signal stability analysis model of the VSM control strategy is proposed. Then, eigenvalue analysis results of the system are presented in section IV. In section V, based on eigenvalue analysis and dynamic simulation, the impacts of the VSM control strategy on SSR are analyzed under different operating conditions, and also compared with that of the conventional VC. Section VI concludes the paper.

II. DFIG-BASED WIND FARM WITH DIFFERENT CONTROL STRATEGIES

A. DFIG-BASED WIND FARM SYSTEM

As shown in Fig. 1, the wind farm in the study system derived from IEEE first benchmark can be represented by an aggregated DFIG model [27]. The stator is directly connected to the set-up transformer T1, which can scale wind turbine capacity (2-MW units) to 890MW by setting the scale factor as 445 [28]. Grid side converter (GSC) is responsible for controlling the DC-link voltage and terminal reactive power. The wind farm is then connected to a 539-kV bus through the set-up transformer T2. In order to reproduce the SSR incident in Texas, the transmission line L2 will be tripped to create a radial connection between the wind farm and the series compensation line L1 [29]. The parameters of the wind farm system can be found in Table 3 in Appendix.

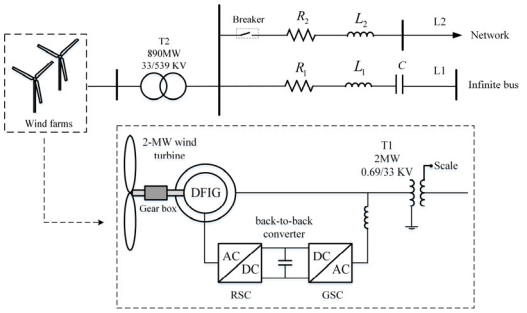

FIGURE 1. Schematic diagram of the DFIG-based wind farm system for SSR study.

B. VIRTUAL SYNCHRONOUS MACHINE CONTROL

The VSM-based control strategy in the RSC was proposed in [7], [8] and has been shown in Fig. 2. The active power imbalance is used to generate the phase angle of rotor voltage θ_r based on the concept of VSM:

$$T_j \frac{d\omega}{dt} = P_m - P_s - D(\omega - \omega_s) \tag{1}$$

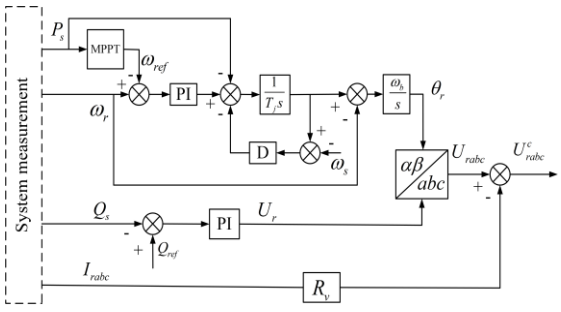

FIGURE 2. Schematic diagram of the virtual synchronous machine (VSM) control for DFIG.

where T_j and D represent the inertia constant and damping coefficient, respectively. P_m is the emulated mechanical power, while P_s is the electrical power. ω_s is the angular frequency of the grid, and ω is the rotating speed of the machine. The reactive power imbalance is used to produce the amplitude of rotor voltage U_r. In this way, the rotor voltage vector U_{rabc} can be generated after coordinate transformation. Note that the phase angle θ_r is varying at a speed of $\omega_s - \omega_r$ in normal state, guaranteeing a synchronous speed of U_{rabc} when the vector is applied to rotor directly. A virtual resistance R_v is then adopted to limit the rotor current transients. U^c_{rabc} is the actual rotor excitation voltage controlled by converters. Compared to conventional VC, the VSM control strategy has been proved superior at providing system appropriate inertial and therefore having an excellent dynamic frequency support ability [7], [8].

C. CONVENTIONAL VC WITH PLL

The configuration of the conventional VC strategy in the RSC is also shown in Fig. 3. Stator-flux oriented control strategy is adopted so that the system can apply decoupled control of active and reactive power. Voltage feed-forward compensation is calculated and added into the control loop. PLL is adopted to calculate the phase angle of terminal voltage θ_{pll}. Stator flux position can be easily achieved due to the fixed phase angle deviation $(\pi/2)$ between the vector of stator voltage and flux where the stator resistance is neglected. The obtained flux phase angle and the measured rotor space angle θ^r_r are used to the coordinate transformation of rotor voltage and current between rotating d-q coordinates and static three-phase coordinates.

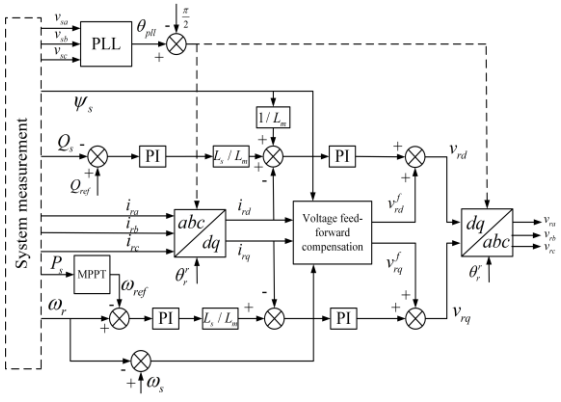

FIGURE 3. Schematic diagram of the conventional vector control (VC) for DFIG.

D. DIFFERENCES BETWEEN THESE TWO CONTROL STRATEGIES

1) REFERENCE FRAME OF THE CONTROL

Different to the fact that VC is established on the rotating d-q reference frame using the PLL, VSM has no oriented vector control. It generates the rotor voltage vector U_{rabc} in polar coordinates and then converts it into a static three phase reference frame. The angular frequency of U_{rabc} is

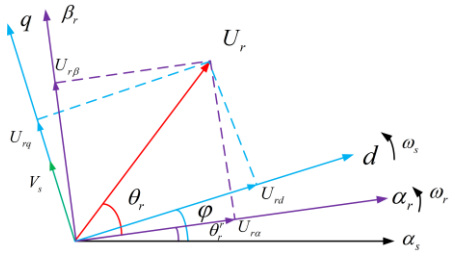

FIGURE 4. Schematic diagram of the rotor voltage vector in the VSM control.

significantly affected by rotor dynamics rather than terminal voltage. The reason is that the generated U_r and θ_r are directly applied to the rotor. Therefore, the rotor excitation voltage can be considered to be decoupled from the terminal stator voltage due to its independent frequency control.

2) CONTROL OF ROTOR CURRENT TRANSIENTS

In the VC, rotor current is completely controlled by the PI controllers in the inner current loop. However, in the VSM, there is only a current limit (R_v) that used to control the rotor current transients. Therefore, the VSM has almost sacrificed the detailed transient control of rotor current, which would result in a worse transient performance.

III. SMALL SIGNAL MODEL FOR VSM CONTROL STRATEGY

A small-signal model of the VSM control strategy is proposed in this section. Note that the generator convention is adopted for the stator current, while the motor convention is adopted for the rotor current. Meanwhile, variables at the equilibrium points are denoted with subscript 0.

Based on Fig. 2, the state space model of the VSM can be described by a fourth-order model as follows:

$$\begin{cases} \dfrac{dx^s_1}{dt} = -\omega_{ref} + \omega_r \\ \dfrac{dx^s_2}{dt} = (k^s_{p1} + \dfrac{k^s_{pi1}}{s})(-\omega_{ref} + \omega_r) - P_s - D(\dfrac{x^s_2}{T_j} - \omega_s) \\ \dfrac{dx^s_3}{dt} = \dfrac{x^s_2}{T_j} - \omega_r \\ \dfrac{dx^s_4}{dt} = Q_{ref} - Q_s \end{cases} \tag{2}$$

where k^s_{p1} and k^s_{pi1} are the proportional and integrating gains of the active power controller, respectively. The output phase angle θ_r and amplitude U_r can be obtained by

$$\begin{cases} \theta_r = \omega_b x^s_3 \\ U_r = (k^s_{q1} + \dfrac{k^s_{qi1}}{s})(Q_{ref} - Q_s) \end{cases} \tag{3}$$

where k^s_{q1} and k^s_{qi1} are the proportional and integrating gains of the reactive power controller, respectively.

Due to the fact that the overall system model is built in a unified d-q coordinates, the generated voltage vector U_{rabc} in polar coordinates needs to be transformed into the unified

d-q coordinates. The relationships of the voltage vector in different coordinates have been illustrated in Fig. 4. The α_r-β_r reference frame is fixed on the rotor and it rotates at the rotor speed ω_r. φ is the angle difference between the rotating d-q and the static reference frame, while θ_r^r refers to the space angle of the rotor. The components $U_{r\alpha}$ and $U_{r\beta}$ can be described as

$$\begin{cases} U_{r\alpha} = U_r \cos\theta_r \\ U_{r\beta} = U_r \sin\theta_r \end{cases} \tag{4}$$

Linearizing (4), we have

$$\begin{bmatrix} \Delta U_{r\alpha} \\ \Delta U_{r\beta} \end{bmatrix} = \begin{bmatrix} \cos\theta_{r0} & -\sin\theta_{r0} \\ \sin\theta_{r0} & \cos\theta_{r0} \end{bmatrix} \begin{bmatrix} \Delta U_r \\ U_{r0}\Delta\theta_r \end{bmatrix} \tag{5}$$

Furthermore, U_{rd} and U_{rq} can be written as

$$\begin{bmatrix} U_{rd} \\ U_{rq} \end{bmatrix} = \begin{bmatrix} \cos(\varphi-\theta_r^r) & \sin(\varphi-\theta_r^r) \\ -\sin(\varphi-\theta_r^r) & \cos(\varphi-\theta_r^r) \end{bmatrix} \begin{bmatrix} U_{r\alpha} \\ U_{r\beta} \end{bmatrix} \tag{6}$$

similarly, (6) can be linearized as

$$\begin{aligned} \begin{bmatrix} \Delta U_{rd} \\ \Delta U_{rq} \end{bmatrix} = & \begin{bmatrix} \cos(\varphi_0-\theta_{r0}^r) & \sin(\varphi_0-\theta_{r0}^r) \\ -\sin(\varphi_0-\theta_{r0}^r) & \cos(\varphi_0-\theta_{r0}^r) \end{bmatrix} \begin{bmatrix} \Delta U_{r\alpha} \\ \Delta U_{r\beta} \end{bmatrix} \\ & - \begin{bmatrix} \sin(\varphi_0-\theta_{r0}^r) & -\cos(\varphi_0-\theta_{r0}^r) \\ \cos(\varphi_0-\theta_{r0}^r) & \sin(\varphi_0-\theta_{r0}^r) \end{bmatrix} \\ & \times \begin{bmatrix} U_{r\alpha 0} \\ U_{r\beta 0} \end{bmatrix} (\Delta\varphi - \Delta\theta_r^r) \end{aligned} \tag{7}$$

Substituting (5) into (7), we have

$$\begin{aligned} \begin{bmatrix} \Delta U_{rd} \\ \Delta U_{rq} \end{bmatrix} = & \begin{bmatrix} \cos(\varphi_0-\theta_{r0}^r-\theta_{r0}) & \sin(\varphi_0-\theta_{r0}^r-\theta_{r0}) \\ -\sin(\varphi_0-\theta_{r0}^r-\theta_{r0}) & \cos(\varphi_0-\theta_{r0}^r-\theta_{r0}) \end{bmatrix} \\ & \times \begin{bmatrix} \Delta U_r \\ U_{r0}\Delta\theta_r \end{bmatrix} - \begin{bmatrix} \sin(\varphi_0-\theta_{r0}^r-\theta_{r0}) \\ \cos(\varphi_0-\theta_{r0}^r-\theta_{r0}) \end{bmatrix} \\ & \times(\Delta\varphi - \Delta\theta_r^r)U_{r0} \end{aligned} \tag{8}$$

where

$$\frac{d\Delta\varphi}{dt} = 0, \quad \frac{d\Delta\theta_r^r}{dt} = \Delta\omega_r \tag{9}$$

It has to be pointed out that the choice of the d-q reference frame here is actually arbitrary since the VSM strategy has no oriented vector control. Therefore, in order to reduce the computational burden, q-axis is fixed on the terminal voltage when system is operating at the equilibrium points.

Considering the rotor current limit, the actual rotor excitation voltage components in the d-q frame is given by

$$\begin{bmatrix} \Delta U_{rd}^c \\ \Delta U_{rq}^c \end{bmatrix} = \begin{bmatrix} \Delta U_{rd} \\ \Delta U_{rq} \end{bmatrix} - R_v \begin{bmatrix} \Delta i_{rd} \\ \Delta i_{rq} \end{bmatrix} \tag{10}$$

Using (2)-(10), the state space model of the VSM can be established.

IV. SMALL SIGNAL STABILITY ANALYSIS

The small-signal stability analysis model for the wind farm system in Fig. 1 can be briefly represented by a 21-order state-space model as follows:

$$\begin{cases} \Delta\dot{X} = A\Delta X + B\Delta Y \\ \Delta Y = C\Delta X + D\Delta Y \end{cases} \tag{11}$$

Y is an vector of the algebraic variables while X contains the state variables of the system as follows:

$$X = \left[X_{line}, X_g, X_{mass}, X_{DC}, X_{RSC}, X_{GSC}\right]^T \tag{12}$$

X_{line} and X_g represent the dynamics of the network and the induction generator, respectively. The two-mass shaft X_{mass} and DC-link X_{DC} can be described by a third-order and a first-order model, respectively. X_{RSC} represents the VSM controller in the RSC from (2) to (10), while X_{GSC} represents the dynamics of the GSC. Eliminating Y, (11) can be rewritten as

$$\Delta\dot{X} = A_{sys}\Delta X \tag{13}$$

where $A_{sys} = A + B(I-D)^{-1}C$. Each complex root of the coefficient matrix A_{sys} represents a system mode $\sigma \pm j\omega$.

For VSM control, the major system modes and their participating states are listed In Table 1, where the wind speed is 9 m/s and the compensation level is 60%. The values of the controller parameters are listed in Table 4 in Appendix. It can be seen that in this case, the SSR mode has a positive real part and the frequency of oscillation is around 37Hz. The SSR mode is not only affected by network dynamics (i_d, i_q, v_{cd}, v_{cq}), but also the voltage behind a transient reactance (e_{ds}, e_{qs}), which are related to the rotor excitation. There is also a super-synchronous resonance (Super-SR) mode, whose frequency is symmetrical to the SSR frequency. Participating factors of these two modes are listed in Table 5 in Appendix. Moreover, it is found that the VSM controller has its own mode, which is related to the state variables x_2^s, x_3^s according to participating factor analysis (around 0.5047 and 0.4991, respectively). This mode has a low frequency and its real part are mainly affected by the value of D and T_j.

TABLE 1. Modes of wind farm with the VSM strategy.

Eigenvalue	Damping ratio	Frequency (Hz)	Participant state	Mode
$-17.74 \pm 513.74j$	0.0345	81.76	i_d, i_q, v_{cd}, v_{cq} $i_{ds}, i_{qs}, e_{ds}, e_{qs}$	Super-SR
$13.18 \pm 236.83j$	–0.0556	37.69	i_d, i_q, v_{cd}, v_{cq} $i_{ds}, i_{qs}, e_{ds}, e_{qs}$	SSR
$-81.55 \pm 60.38j$	0.8037	9.61	$i_{ds}, i_{qs}, e_{ds}, e_{qs}$	Electro-mechanical
$-1.94 \pm 8.05j$	0.2343	1.28	x_2^s, x_3^s	VSM-controller

In order to have a better understanding, modes from the VC-based system in the same scenario are provided in Table 2. The detailed mathematic model of the wind farm with VC strategy can be found in [30]. It can be seen that the shaft mode is only related to its own shaft dynamics ω_t, θ_{tw}, ω_r and its frequency is close to that of the VSM-controller mode. The SSR mode has a smaller real part and the frequency of oscillation is close to that in the wind farm with VSM. Besides, it is found that the PLL in the VC has its own mode and does not have major effects on the SSR mode (around 0.0008).

TABLE 2. Modes of wind farm with the VC strategy.

Eigenvalue	Damping ratio	Frequency (Hz)	Participant state	Mode
$-15.24 \pm 509.89\,j$	0.0299	81.00	i_d, i_q, v_{cd}, v_{cq} $i_{ds}, i_{qs}, e_{ds}, e_{qs}$	Super-SR
$6.002 \pm 243.77\,j$	−0.0246	38.79	i_d, i_q, v_{cd}, v_{cq} $i_{ds}, i_{qs}, e_{ds}, e_{qs}$	SSR
$-56.39 \pm 40.07\,j$	0.8151	6.37	$i_{ds}, i_{qs}, e_{ds}, e_{qs}$	Electro-mechanical
$-3.01 \pm 12.23\,j$	0.2385	1.94	$\omega_t, \theta_{tw}, \omega_r$	Shaft
$-24.93 \pm 16.61\,j$	0.8322	2.64	x_{pll}, θ_{pll}	PLL

V. COMPARISON OF TWO CONTROL STRATEGIES ON SSR MODE

In this section, dynamics of SSR in the VSM-based wind farm are analyzed further under different conditions, and compared to those in the wind farm with the conventional VC.

A. UNDER DIFFERENT SERIES COMPENSATION LEVELS

It is well known that the series compensation level, which can be represented by k, is one of the major factors that significantly affect the SSR mode. In Fig. 5, responses of the wind farm active power under different compensation levels (60%, 40% and 20%) at a fixed wind speed ($V_m = 9$ m/s) are shown. Meanwhile, results of the Fast Fourier Transform (FFT) analysis of each oscillation are presented in Fig. 6. For the two strategies, it can be observed that with the series compensation level decreased, oscillation frequency becomes greater, while the corresponding amplitude is gradually reduced. When at a same compensation level, e.g., 40%, the oscillation amplitude of the wind farm with VSM is greater than that of the wind farm with VC, indicating a weaker damping. Particularly, it is noticed that when the compensation level is decreased to 20%, the VC-based system becomes stable and SSR will not happen anymore, while the VSM-based system still suffers from SSR. These FFT and simulation results indicate that the wind farm with VSM control has a worse performance than the wind farm with VC at same compensation levels.

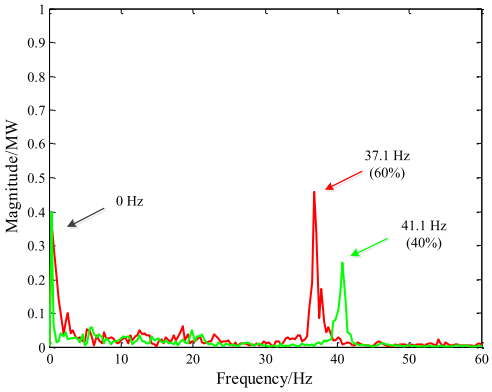

(a) Spectrum of active power in wind farm with VC

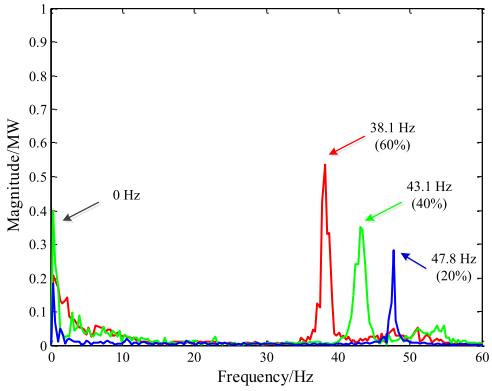

(b) Spectrum of active power in wind farm with VSM

FIGURE 6. Results of FFT analysis: (a) in wind farm with VC and (b) in wind farm with VSM.

The above conclusion can also be verified by eigenvalue analysis. Movements of the SSR mode under different compensation levels are shown in Fig. 7. It can be seen that with the compensation level increased from 1% to 80%, the SSR mode of the wind farm with the two strategies moves towards

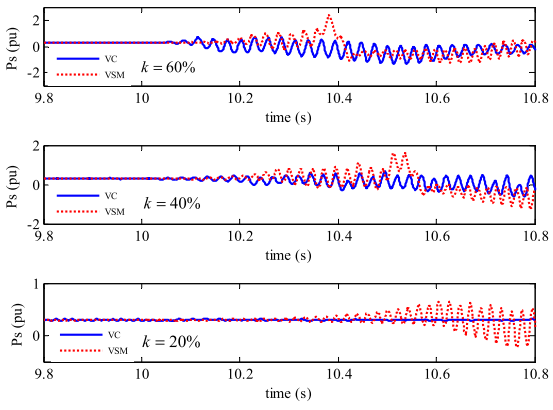

FIGURE 5. Responses of active power under different compensation levels.

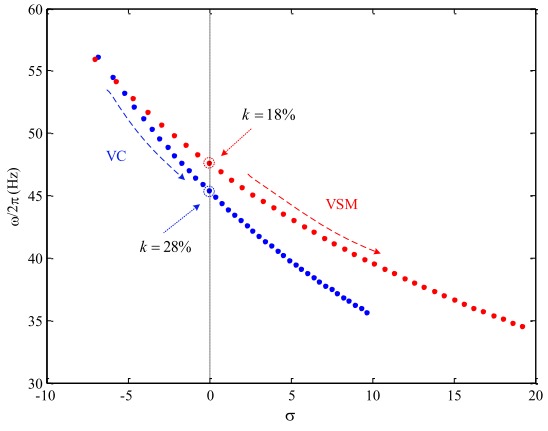

FIGURE 7. Movements of SSR mode under different series compensation levels.

the right-half plane. When beyond a critical point (around 28% and 18% respectively), the mode goes into the right half-plane and the system is not stable any more. Obviously, it can be found that the mode of the wind farm with VSM moves faster than that of the wind farm with VC, indicating a weaker damping and a higher sensitivity to compensation levels. All of these comparisons demonstrate the worse performance of VSM strategy on SSR, which is consistent with the simulation results.

B. UNDER DIFFERENT CONTROLLER PARAMETERS

For the VSM control, movements of the SSR mode under different values of T_j, k^s_{q1}, k^s_{qi1} and R_v are shown in Fig. 8, where $V_m = 9$ m/s and $k = 60\%$. The impacts of k^s_{p1}, k^s_{pi1} and D are not presented in this figure because when their values are changed, SSR mode almost remains relatively motionless. Therefore, they can be considered as having little effect on the SSR mode. It can be seen from the figure that T_j and k^s_{qi1} affect the mode slightly while k^s_{q1} can move the mode to the right-hand side quickly when it is increased from 0.1 to 1. The SSR mode can locates at the left half-plane when R_v is decreased from 1.5 to 0.1. Moreover, it is noticed that the oscillation frequency can be changed with the variation of R_v and k^s_{q1}. The reason is that the converters in DFIG act as 'inductive or capacitive reactance' under different parameter values, ultimately resulting in a change of system resonant frequency.

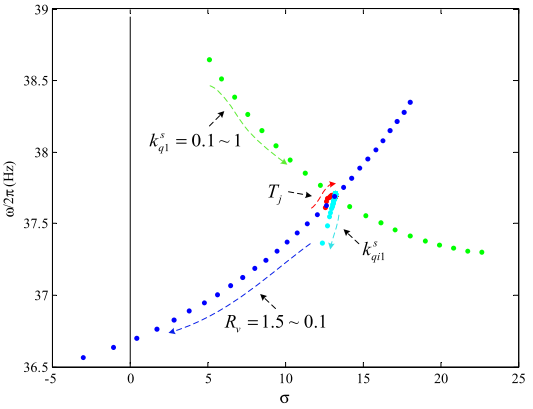

FIGURE 8. Movements of SSR mode based on different parameters in the VSM.

In order to further study the impacts of R_v and k^s_{q1}, and find out the SSR stable area, a three-dimensional diagram with the real part of eigenvalue σ as z-axis is provided in Fig. 9. It can be seen that the surface is divided into a stable and an unstable area by a zero-plane when varying R_v and k^s_{q1} from 0.1 to 1.5 and 0.1 to 2 respectively. The SSR is expected to be avoided when selecting the values of R_v and k^s_{q1} from the stable area.

This conclusion can be confirmed by simulations in Fig. 10 (a). It can be seen that when the parameters are chosen from the stable area, e.g. $R_v = 0.15$ and $k^s_{q1} = 0.5$, the system is stable and SSR doesn't happen. However, with

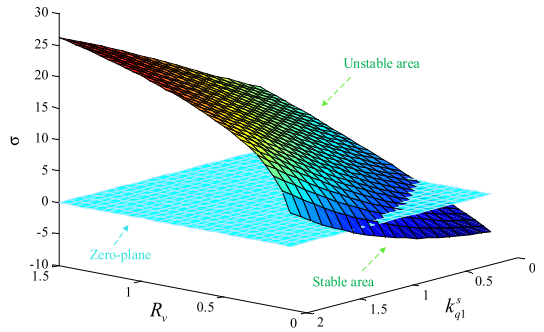

FIGURE 9. Movements of SSR mode under different R_v and k^s_{q1}.

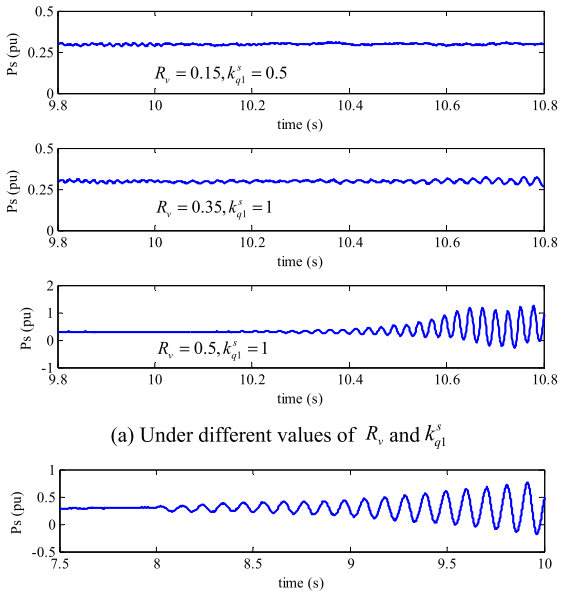

(a) Under different values of R_v and k^s_{q1}

(b) A step change of R_v from 0.1 to 0.08 at 8s

FIGURE 10. Responses of the active power under different R_v and k^s_{q1}.

the selected parameters close to the unstable area, the wind farm becomes weaker. Till the parameters are chosen from the unstable area, SSR is triggered.

It is known that R_v is designed to limit the rotor current transients. The smaller the value of R_v, the weaker the control of rotor current. When R_v decreases to an enough small value, the control system will become unstable. For example, when a small change of R_v from 0.1 to 0.08 happens at 8s in Fig. 10 (b), the wind farm system is out of control. Therefore, the adjusting range of R_v exists limitations.

For the conventional VC, results become different. There are three parameters that have significant impacts on the SSR mode according to Fig. 11. k_{p2}, k_{q1} and k_{q2} are the proportional gains of active and reactive power controllers, respectively. When they are increased from 0.1 to 4, the SSR mode is moved to the right greatly, and k_{q1} and k_{q2} obviously make the mode move faster than k_{p2}. The oscillation frequency also becomes greater with the increase of k_{p2}, k_{q1} and k_{q2}. Moreover, it can be seen that k_{p2}, k_{q1} and k_{q2} have

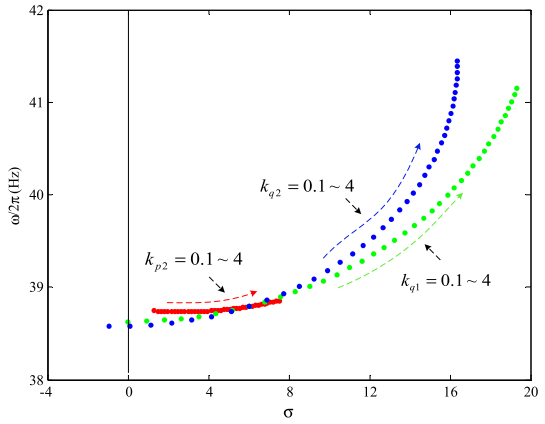

FIGURE 11. Movements of SSR mode under different PI controller parameters.

the capability to make the mode locate at the left half-plane. Therefore, another three-dimensional diagram with the same z-axis is shown in Fig. 12, where k_{q1} and k_{q2} in the range of 0.1 and 2 are set as the x-axis and y-axis respectively. Similarly, stable and unstable areas divided by a zero-plane can also be observed. When another parameter k_{p2} is changed between 0.2 and 3.5, the surfaces gradually move up or down and the size of the stable areas changes as well. Simulation results in Fig. 13 are presented to verify the eigenvalue analysis results. SSR is easily triggered in the first curves, where the parameters are chosen from the unstable area. With the selected parameters move close to the stable area, the oscillations become weaker. Till the parameters are chosen from the stable area, e.g., $k_{p2} = 1 k_{q1} = 0.3$ and $k_{q2} = 0.3$, the system indeed becomes stable.

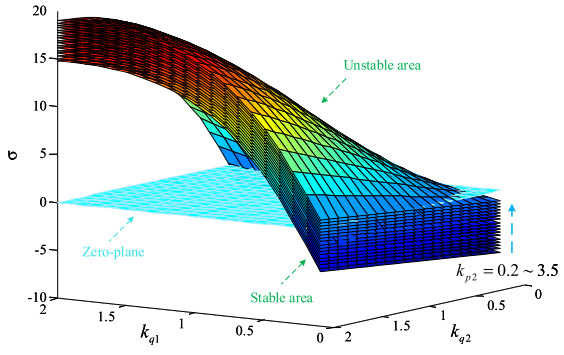

FIGURE 12. Movements of SSR mode under different k_{p2}, k_{q1} and k_{q2}.

The above eigenvalue analysis and simulation results have confirmed that there are three parameters in the VC and only two in the VSM that can be regulated to avoid SSR. The adjusting range of virtual resistance R_v in the VSM has limitations. By contrast, the SSR stable areas in the VC-based system are more flexible due to their wider adjusting range.

It should be pointed out that R_v are related to the control of the rotor current, whose dynamics significantly affect the SSR. The VC has a more control capability for rotor current

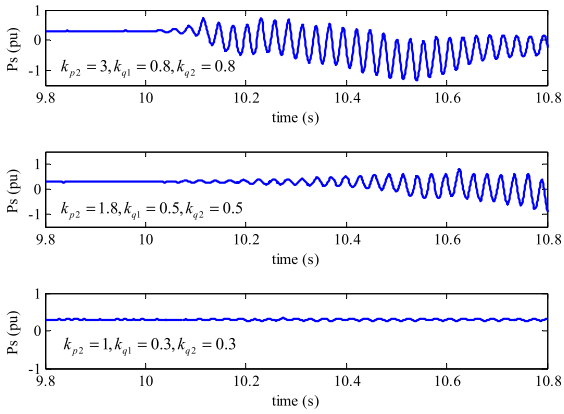

FIGURE 13. Responses of active power under different k_{p2}, k_{q1} and k_{q2}.

than the VSM, which mainly contributes to its better performance on SSR mitigation by adjusting controller parameters.

C. UNDER DIFFERENT WIND SPEEDS

Wind speed is another factor that significantly affects the SSR mode. Dynamic responses of the active power under different wind speeds (9 m/s, 10.5 m /s and 12 m/s) based on VSM and VC strategies are shown in Fig. 14, respectively, where $k = 60\%$. It can be seen that at the same wind speed, e.g., 9 m/s, the power fluctuation range of the wind farm with VSM are greater than that of the wind farm with VC. With wind speed increased from 9 m/s to 12 m/s, the system damping is lightly increased and the oscillation frequency is decreased. When wind speed approaches 12 m/s, the wind farm system with VC becomes stable and no oscillation happens any more. By contrast, for the VSM control strategy, even if the wind speed is 12, the system still suffers from SSR. These simulation results suggest that with the same wind speed, the VC-based system can perform better than the VSM-based system in terms of SSR.

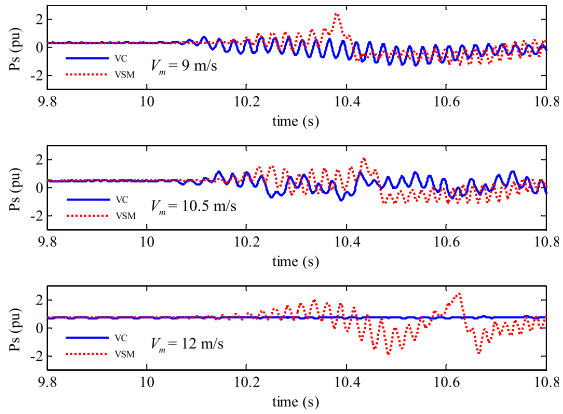

FIGURE 14. Responses of the active power under different wind speeds.

Same conclusion can also be drawn according to the eigenvalue analysis. Movements of the SSR mode based on these two strategies are illustrated in Fig. 15. It can be seen that

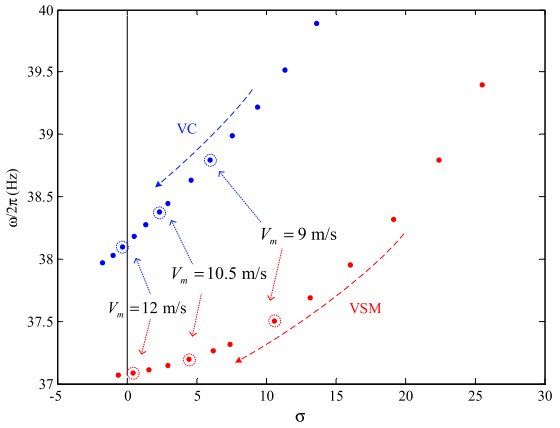

FIGURE 15. Movements of SSR mode under different wind speeds based on VC and VSM strategy.

with the wind speed increased from 7 m/s to 13 m/s, the real part of the eigenvalue and oscillation frequency of the SSR mode are decreased. Meanwhile, the SSR mode in the VC-based system will locate at the left-half plane when the wind speed approaches around 12 m/s, while the modes in the VSM-based system are still at the right-half plane.

VI. CONCLUSION

The dynamics of SSR in VSM-based wind farms under different operational conditions were analyzed in this paper by conducting eigenvalue analysis and dynamic simulations. Compared to conventional VC, it was found that SSR is more likely to be triggered in wind farms with VSM when at a same compensation level. Besides, there are mainly two controller parameters in the VSM that can be used to avoid SSR, and the adjusting range of these two parameters has limitations. When wind speed increases to 12 m/s, SSR can be triggered in the VSM-based system, but does not happen in the VC-based wind farms. These analysis results have confirmed better performance of VC than VSM in terms of SSR in DFIG-based wind farms. This is because VSM has almost sacrificed the detailed transient control of the rotor current. More research efforts on the impacts of VSM on SSR in other applications, such as HVDC transmission systems and PMSG-based wind energy systems, etc. are needed.

TABLE 3. Parameters of network and DFIG.

Network Parameters	Variable	Value
Line 1 resistance	R_1	6.471 *ohm*
Line 1 inductance	L_1	0.1014 *H*
Line 1 capacitor ($k = 60\%$)	C	115.6 μF
Line 2 resistance	R_2	0.001 *ohm*
Line 2 inductance	L_2	0.1 *H*
T1 leakage inductance (0.69/33 kV)	L_{T1}	0.1 *pu*
T2 leakage inductance (33/539 kV)	L_{T2}	0.1 *pu*
Generator Parameters	**Variable**	**Value**
Rated power	P_{base}	2 MW
Rated voltage	V_{base}	0.69 kV
Stator resistance	r_s	0.00488 *pu*
Rotor resistance	r_r	0.00549 *pu*
Stator leakage inductance	L_s	0.09231 *pu*
Rotor leakage inductance	L_r	0.09955 *pu*
Magnetizing inductance	L_m	3.95279 *pu*

APPENDIX

See Tables 3–5.

TABLE 4. Parameters of the controller in VC and VSM.

	Controller Parameters
VC	$k_{p1}=3, k_{pi1}=1/0.3 \quad k_{p2}=3, k_{pi2}=1/0.1$
	$k_{q1}=0.8, k_{qi1}=1/0.5 \quad k_{q2}=0.8, k_{qi2}=1/0.1$
VSM	$k^s_{p1}=3, k^s_{pi1}=1/0.8$
	$k^s_{q1}=1, k^s_{qi1}=1/0.25$
	$D=50, T_j=10, R_v=1$

TABLE 5. Participating factors of modes in VSM and VC.

	VSM			VC		
State Variable	SSR	Super-SR	Electro-mechanical	SSR	Super-SR	Electro-mechanical
i_d, i_q	0.1130 0.1154	0.1500 0.1618	0.0497 0.1669	0.1384 0.1335	0.1558 0.1516	0.0368 0.0493
v_{cd}, v_{cq}	0.1807 0.1776	0.2188 0.2220	0.0344 0.0195	0.2132 0.2038	0.2410 0.2302	0.0135 0.0117
i_{ds}, i_{qs}	0.0584 0.0848	0.0772 0.1032	0.0315 0.0966	0.0722 0.0770	0.0832 0.0937	0.0254 0.0323
e_{ds}, e_{qs}	0.1189 0.1116	0.0323 0.0274	0.3121 0.2822	0.0643 0.0866	0.0138 0.0207	0.3473 0.4743

REFERENCES

[1] *Global Wind Report 2018*, GWEC, Brussels, Belgium, 2019.

[2] H.-P. Beck and R. Hesse, "Virtual synchronous machine," in *Proc. 9th Int. Conf. Elect. Power Quality Utilisation*, Oct. 2007, pp. 1–6.

[3] J. Liu, Y. Miura, and T. Ise, "Comparison of dynamic characteristics between virtual synchronous generator and droop control in inverter-based distributed generators," *IEEE Trans. Power Electron.*, vol. 31, no. 5, pp. 3600–3611, May 2016.

[4] K. Visscher and S. W. H. De Haan, "Virtual synchronous machines (VSG's) for frequency stabilisation in future grids with a significant share of decentralized generation," in *Proc. Smart Grids Distrib.*, Jun. 2008, pp. 1–4.

[5] Q.-C. Zhong, Z. Ma, W.-L. Ming, and G. C. Konstantopoulos, "Grid-friendly wind power systems based on the synchronverter technology," *Energy Convers. Manage.*, vol. 89, pp. 719–726, Jan. 2015.

[6] Y. Ma, W. Cao, L. F. Yang, F. Wang, and L. M. Tolbert, "Virtual synchronous generator control of full converter wind turbines with short-term energy storage," *IEEE Trans. Ind. Electron.*, vol. 64, no. 11, pp. 8821–8831, Nov. 2017.

[7] S. Wang, J. Hu, and X. Yuan, "Virtual synchronous control for grid-connected DFIG-based wind turbines," *IEEE J. Emerg. Sel. Topics Power Electron.*, vol. 3, no. 4, pp. 932–944, Dec. 2015.

[8] S. Wang, J. Hu, X. Yuan, and L. Sun, "On inertial dynamics of virtual-synchronous-controlled DFIG-based wind turbines," *IEEE Trans. Energy Convers.*, vol. 30, no. 4, pp. 1691–1702, Dec. 2015.

[9] R. Aouini, B. Marinescu, K. B. Kilani, and M. Elleuch, "Synchronverter-based emulation and control of HVDC transmission," *IEEE Trans. Power Syst.*, vol. 31, no. 1, pp. 278–286, Jan. 2016.

[10] J. Liu, D. Yang, W. Yao, R. Fang, H. Zhao, and B. Wang, "PV-based virtual synchronous generator with variable inertia to enhance power system transient stability utilizing the energy storage system," *Protection Control Mod. Power Syst.*, vol. 2, no. 1, Nov. 2017, Art. no. 39.
[11] C. Li, R. Burgos, I. Cvetkovic, D. Boroyevich, L. Mili, and P. Rodriguez, "Analysis and design of virtual synchronous machine based STATCOM controller," in *Proc. IEEE 15th Workshop Control Modeling Power Electron. (COMPEL)*, Jun. 2014, pp. 1–6.
[12] B. Liu, Z. Li, X. Chen, Y. Huang, and X. Liu, "Recognition and vulnerability analysis of key nodes in power grid based on complex network centrality," *IEEE Trans. Circuits Syst., II, Exp. Briefs*, vol. 65, no. 3, pp. 346–350, Mar. 2018.
[13] P. Pourbeik, R. Koessler, D. L. Dickmander, and W. Wong, "Integration of large wind farms into utility grids (part 2-performance issues)," in *Proc. IEEE Power Eng. Soc. Gen. Meeting*, Jul. 2003, pp. 1520–1525.
[14] L. C. Gross, "Sub-synchronous grid conditions: New event new problem and new solutions," in *Proc. 37th Annu. Western Protective Relay Conf.*, Spokane, WA, USA, 2010, pp. 1–19.
[15] K. Narendra, D. Fedirchuk, R. Midence, N. Zhang, A. Mulawarman, P. Mysore, and V. Sood, "New microprocessor based relay to monitor and protect power systems against sub-harmonics," in *Proc. IEEE Elect. Power Energy Conf.*, Winnipeg, MB, Canada, Oct. 2011, pp. 438–443.
[16] L. Wang, X. Xie, H. Liu, Y. Zhan, J. He, and C. Wang, "Review of emerging SSR/SSO issues and their classifications," *J. Eng.*, vol. 2017, no. 13, pp. 1666–1670, Oct. 2017.
[17] L. Wang, X. Xie, Q. Jiang, H. Liu, Y. Li, and H. Liu, "Investigation of SSR in practical DFIG-based wind farms connected to a series-compensated power system," *IEEE Trans. Power Syst.*, vol. 30, no. 5, pp. 2772–2779, Sep. 2015.
[18] W. Chen, X. Xie, D. Wang, H. Liu, and H. Liu, "Probabilistic stability analysis of subsynchronous resonance for series-compensated DFIG-based wind farms," *IEEE Trans. Sustain. Energy*, vol. 9, no. 1, pp. 400–409, Jan. 2017.
[19] H. Liu, X. Xie, X. Gao, H. Liu, and Y. Li, "Stability analysis of SSR in multiple wind farms connected to series-compensated systems using impedance network model," *IEEE Trans. Power Syst.*, vol. 33, no. 3, pp. 3118–3128, May 2017.
[20] M. Wu, L. Xie, L. Cheng, and R. Sun, "A study on the impact of wind farm spatial distribution on power system sub-synchronous oscillations," *IEEE Trans. Power Syst.*, vol. 31, no. 3, pp. 2154–2162, May 2016.
[21] A. E. Leon, "Integration of DFIG-based wind farms into series-compensated transmission systems," *IEEE Trans. Sustain. Energy*, vol. 7, no. 2, pp. 451–460, Apr. 2016.
[22] P.-H. Huang, M. S. El Moursi, W. Xiao, and J. L. Kirtley, "Subsynchronous resonance mitigation for series-compensated DFIG-based wind farm by using two-degree-of-freedom control strategy," *IEEE Trans. Power Syst.*, vol. 30, no. 3, pp. 1442–1454, May 2015.
[23] T. Rajaram, J. M. Reddy, and Y. Xu, "Kalman filter based detection and mitigation of subsynchronous resonance with SSSC," *IEEE Trans. Power Syst.*, vol. 32, no. 2, pp. 1400–1409, Mar. 2017.
[24] H. A. Mohammadpour, M. M. Islam, E. Santi, and Y.-J. Shin, "SSR damping in fixed-speed wind farms using series FACTS controllers," *IEEE Trans. Power Del.*, vol. 31, no. 1, pp. 76–86, Feb. 2016.
[25] X. Liu, L. Li, Z. Li, X. Chen, T. Fernando, H. H.-C. Iu, and G. He, "Event-trigger particle filter for smart grids with limited communication bandwidth infrastructure," *IEEE Trans. Smart Grid*, vol. 9, no. 6, pp. 6918–6928, Nov. 2018.
[26] S. Li, L. Li, Z. Li, X. Chen, T. Fernando, H. H.-C. Iu, G. He, Q. Wang, and X. Liu, "Event-trigger heterogeneous nonlinear filter for wide-area measurement systems in power grid," *IEEE Trans. Smart Grid*, vol. 10, no. 3, pp. 2752–2764, May 2019.
[27] I. S. W. Group, "First benchmark model for computer simulation of subsynchronous resonance," *IEEE Trans. Power App. Syst.*, vol. PAS-96, no. 5, pp. 1565–1572, Sep. 1977.
[28] B. Massimo, P. Andreas, and A. Evert, *The Impact of Wind Farms on Sub-Synchronous Resonance in Power Systems*. Stockholm, Sweden: ELFORSK, 2011.
[29] A. E. Leon and J. A. Solsona, "Sub-synchronous interaction damping control for DFIG wind turbines," *IEEE Trans. Power Syst.*, vol. 30, no. 1, pp. 419–428, Jan. 2015.
[30] F. Wu, X. P. Zhang, K. Godfrey, and P. Ju, "Small signal stability analysis and optimal control of a wind turbine with doubly fed induction generator," *IET Gener., Transmiss. Distrib.*, vol. 1, no. 5, pp. 751–760, Sep. 2007.

KANGHUI GU received the B.Eng. degree in electrical engineering from the Jiangsu University of Science and Technology, China, in 2014. He is currently pursuing the the Ph.D. degree in electrical engineering with Hohai University. His research interests include modeling and stability analysis of renewable energy generation.

FENG WU received the B.Eng. and M.Sc. degrees in electrical engineering from Hohai University, China, in 1998 and 2002, respectively, and the Ph.D. degree in electrical engineering from the University of Birmingham, U.K., in 2009. He is currently a Professor with Hohai University. His research interest includes the modeling and the control of renewable energy generation.

XIAO-PING ZHANG (M'95–SM'06) received the B.Eng., M.Sc., and Ph.D. degrees in electrical engineering from Southeast University, China, in 1988, 1990, and 1993, respectively. He was an Associate Professor with the University of Warwick, U.K. He was with China State Grid EPRI (NARI Group) on EMS/DMS advanced application software research and development, from 1993 to 1998. From 1998 to 1999, he was visiting UMIST. From 1999 to 2000, he was an Alexander-von-Humboldt Research Fellow of the University of Dortmund, Germany. He is currently a Professor of electrical power systems with the University of Birmingham, U.K., and he is also the Director of smart grid with the Birmingham Energy Institute and the Co-Director of the Birmingham Energy Storage Center. He has coauthored the first and second edition of the monograph *Flexible AC Transmission Systems: Modeling and Control* (Springer, in 2006 and 2012). He has coauthored the book *Restructured Electric Power Systems: Analysis of Electricity Markets with Equilibrium Models* (IEEE Press/Wiley, 2010). He is an Advisor of the IEEE PEs, U.K., and Ireland Chapter.

PING JU (M'95–SM'10) received the B.S. and M.S. degrees in electrical engineering from Southeast University, Nanjing, China, in 1982 and 1985, respectively, and the Ph.D. degree in electrical engineering from Zhejiang University, Hangzhou, China. He is currently a Professor of electrical engineering with Hohai University, Nanjing, China, and Zhejiang University. From 1994 to 1995, he was an Alexander-von-Humboldt Fellow of the University of Dortmund, Germany. His research interests include the modeling and the control of power system with integration of renewable generation.

HAIQIANG ZHOU received the Ph.D. degree in electrical engineering from Zhejiang University, Hangzhou, China, in 2003. Since 2003, he has been with Hohai University, Nanjing, China, where he became a Professor. His research interests include large scale power system modeling and stability analysis.

JIAJIE LUO was born in Guangdong, China, in 1993. He received the B.Eng. degrees from the Huazhong University of Science and Technology, Wuhan, China, and from the University of Birmingham, Birmingham, U.K., in 2015, where he is currently pursuing the Ph.D. degree. His research interests include renewable energy integration, modeling, and control.

JIANING LI (S'15–M'17) received the B.Eng. degrees in electrical and electronic engineering from the Huazhong University of Science and Technology, China, and from the University of Birmingham, U.K., in 2011, and the Ph.D. degree from the School of Electronic, Electrical and Systems Engineering, University of Birmingham, U.K., in 2016, where he is currently a Senior Research Fellow of power systems. His research interests include renewable energy systems and smart grid technology.